Nanoscale

RSC Publishing

PAPER

View Article Online
View Journal | View Issue

Published on 14 May 2013. Downloaded by Shanghai Jiaotong University on 01/11/2013 10:41:38.

Cite this: *Nanoscale*, 2013, **5**, 5489

Silica/titania sandwich-like mesoporous nanosheets embedded with metal nanoparticles templated by hyperbranched poly(ether amine) (hPEA)†

Bing Yu, Xuesong Jiang* and Jie Yin

We here demonstrated a novel square silica/titania mesoporous nanosheet which was prepared with hyperbranched poly(ether amine) nanosheets (hPEA-NSs) as a template. TEM and SEM images reveal that the obtained nanosheets possess a large aspect ratio with the average edge length of 1–2 μm and thickness of ~40 nm, respectively. Various metal nanoparticles such as gold, silver, and platinum can be embedded into these nanosheets with hPEA-NSs decorated with the corresponding nanoparticles as templates. These nanosheets possess a sandwich-like structure, which is comprised of amorphous SiO_2 as the inner layer, and the anatase TiO_2 as the outer layer determined by a cross-sectional STEM image and EDS mapping. Meanwhile, the obtained nanosheets are mesoporous with a high surface area (~429 $m^2\ g^{-1}$), and the SiO_2 inner layer can be removed by chemical etching with NaOH solution to obtain anatase TiO_2 nanosheet-like boxes embedded with gold nanoparticles (AuNPs). The photodegradation of Methyl Orange (MO) by the obtained nanosheets can be enhanced by the embedding of AuNPs owing to the localized surface plasmon resonance (LSPR) effect from AuNPs. The preparation of a silica/titania mesoporous nanosheet with hPEA-NSs as template is believed to provide a convenient and general method to produce various square inorganic mesoporous nanosheets with a large aspect ratio between edge length and thickness.

Received 18th March 2013
Accepted 7th April 2013

DOI: 10.1039/c3nr01336g

www.rsc.org/nanoscale

Introduction

Recently, two-dimensional (2D) nanomaterials of nanoscale dimensions in thickness only and a relatively large length in the plane, have attracted tremendous attention as a result of their unique magnetic, electronic and storage properties, and potential applications in the areas of electronics, sensors, as well as energy storage and conversion.[1–5] Varieties of 2D materials, such as MoS_2 nanoflakes,[6] WO_3 nanoplates,[7] CeO_2 nanoplates,[8] PbS nanosheets,[9] MnO_2 nanosheets,[10] SnS_2 nanosheets,[11] FeS_2 nanosheets,[12] and GaS nanosheets[13] have been successfully synthesized. However, more kinds of 2D materials, especially multi-component 2D materials, are required as a result of their variety of application. Accordingly, it is significant to develop an efficient and general method to synthesize various 2D inorganic materials.

Inorganic materials with different nanostructures have been prepared by using different templates, including silica spheres,[14] self-assembled polymers,[15–18] carbon materials (carbon nanotubes or graphene),[19,20] biological superstructures (amino acid, viruses or DNA),[21–23] and even natural leaves[24] and butterfly wings.[25] Varieties of inorganic materials such as TiO_2,[26] SiO_2,[27] CdS,[28] CdSe,[29] ZnO,[30] Nb_2O_5,[31] GeO_2,[31] and ZrO_2[31] with different nanostructures can be fabricated with polymer templating methods. The obtained inorganic materials often possess a hollow and mesoporous structure depending on the structure of the template polymers. Although the inorganic nanosheets were successfully prepared by using graphene oxide (GO) and reduced graphene oxide (RGO) nanosheets as templates,[32,33] the preparation of 2D inorganic materials with the polymer templating method has been rather less reported, which might be due to difficulties in fabrication of the functional polymer nanosheets.[34]

Recently, polymer nanosheets (hPEA-NSs) with edge lengths of 1–2 μm and an ultrathin thicknesses of 4–5 nm have been developed by our group through self-assembly of hyperbranched poly(ether amine) (hPEA) ended with polyhedral oligomeric silsesquioxane (POSS) and anthracene (AN).[35] The obtained hPEA-NSs possess a sandwich-like structure, which is comprised of the hydrophilic outer layer of hPEA and the hydrophobic crosslinked inner layer of POSS and AN moieties. Owing to existence of amino groups and poly(ethylene oxide) (PEO) short chains on the outer layer of hPEA-NSs, similar to reported polymer templates, inorganic precursors can also be immobilized on the surface of the nanosheet. As a result,

School of Chemistry & Chemical Engineering, State Key Laboratory for Metal Matrix Composite Materials, Shanghai Jiao Tong University, Shanghai 200240, People's Republic of China. E-mail: ponygle@sjtu.edu.cn; Fax: +86-21-54747445; Tel: +86-21-54743268

† Electronic supplementary information (ESI) available. See DOI: 10.1039/c3nr01336g

Published on 14 May 2013. Downloaded by Shanghai Jiaotong University on 01/11/2013 10:41:38.

hPEA-NSs can be expected as templates to prepare various 2D inorganic materials. Meanwhile, our recent study shows that hPEA-NSs can be used as platforms for various metal nanoparticles (Au, Ag, Pt), which could be decorated on hPEA-NSs through *in situ* reduction of the corresponding precursors adsorbed on the surface of the hPEA-NSs through complexation effects.[36] Therefore, different kinds of metal nanoparticles could be embedded into the obtained inorganic nanosheets with a one-step method by using hPEA-NSs templates decorated with the corresponding metal nanoparticles.

Herein, we report 2D inorganic materials of the silica/titania mesoporous nanosheets (SiO_2/TiO_2-NSs), prepared by using hPEA-NSs as templates. As one of the most useful semiconducting metal oxides, titania (TiO_2) has attracted much attention for its applications in various areas, such as photocatalytic degradation[37] and hydrogen generation,[38] electrocatalysis,[39] dye-sensitized solar cells,[40] lithium ion batteries,[41] self-cleaning,[42] and so on. We here use SiO_2/TiO_2-NSs as an example for the preparation of 2D inorganic materials with hPEA-NSs as templates. The obtained SiO_2/TiO_2-NSs possess a sandwich-like structure with a thickness of ~40 nm, which is comprised of amorphous SiO_2 as the inner layer and anatase TiO_2 as the outer layer. Gold, silver, and platinum nanoparticles can be embedded into these SiO_2/TiO_2-NSs with the hPEA-NSs templates decorated with the corresponding metal nanoparticles. The obtained SiO_2/TiO_2-NSs possess high surface areas (~429 $m^2 g^{-1}$) and total pore volumes (~0.53 $cm^3 g^{-1}$). The SiO_2 inner layer of the obtained nanosheets embedded with gold nanoparticles (AuNPs) can be removed by chemical etching with NaOH solution to obtain anatase TiO_2 nanosheet-like boxes embedded with AuNPs. The photocatalytic activities of the obtained nanosheets can be enhanced by embedding AuNPs. It is apparent that the preparation of silica/titania mesoporous nanosheets with hPEA-NSs as template could be further extended to fabricate a variety of mesoporous metal and metal oxide sheets, thus this strategy opens up a unique opportunity for the general production of square inorganic mesoporous nanosheets with high surface areas, thin thickness, and a large aspect ratio between edge length and thickness.

Experimental

Materials

Tetraethoxysilane (TEOS), titanium(IV) tetra-*n*-butoxide (TBT), tetrachloroauric(III) acid ($HAuCl_4$), silver nitrate ($AgNO_3$) and hexachloroplatinic(IV) acid (H_2PtCl_6) were all purchased from Sinopharm Chemical Reagent and used without purification. POSS/AN-ended hyperbranched poly(ether amine) (**HPA**) was synthesized in our lab according to a previous report,[35] while the mole ratio of POSS and AN moieties in **HPA** is 1/1. Other chemicals are of analytical grade except as noted.

Preparation of silica nanosheets (SiO_2-NSs) templated by HPA nanosheets (hPEA-NSs)

According our previous report, hPEA-NSs could be obtained by self-assembly of POSS/AN-ended hyperbranched poly(ether amine) (**HPA**), and the procedure is listed in the literature.[35] TEOS (2.08 g, 0.01 mol) was dissolved into 10 mL 0.01 mol L^{-1} HCl–ethanol (1 : 1, v/v) and the mixture was stirred for 30 min at room temperature, then TEOS solution was obtained. Meanwhile, 1 mL of pH 7.4 phosphate buffered saline (PBS) was added into 6 mL 1 mg mL^{-1} hPEA-NSs aqueous dispersion, then 0.15 mL of the TEOS solution prepared above was slowly added, and the mixture was stirred for 24 h. The hydrolysis of TEOS on hPEA-NSs under the catalysis of amino groups resulted in the formation of the SiO_2-NSs. The suspended SiO_2-NSs were collected by centrifugation and washed with deionized water and ethanol, respectively, and then dried in vacuum for 12 h at room temperature. SiO_2-NSs embedded with gold, silver and platinum nanoparticles could be prepared similarly with Au@hPEA-NSs, Ag@hPEA-NSs, and Pt@hPEA-NSs as templates, respectively, and the procedure to prepare hPEA-NSs decorated with these nanoparticles is according to our previous research.[36]

Preparation of silica/titania nanosheets (SiO_2/TiO_2-NSs)

TBT (3.40 g, 0.1 mol) was dissolved into 10 mL ethanol. Meanwhile, the as-prepared SiO_2-NSs (ap-SiO_2-NSs) were dispersed into 6 mL ethanol, then the 0.2 mL TBT ethanol solution prepared above was slowly added, and the mixture was stirred for 24 h. The hydrolysis of TBT on SiO_2-NSs under the catalysis of amino groups in hPEA-NSs resulted in the formation of the SiO_2/TiO_2-NSs, which were collected by centrifugation and washed with deionized water and ethanol, respectively, and then dried in vacuum for 12 h at room temperature. The hPEA-NSs template was removed by calcination by heating in air at 3 °C min^{-1} to 300 °C and maintaining this temperature for 3 h, and then to 600 °C at a rate of 3 °C min^{-1}, while the amorphous TiO_2 in the nanosheets partly crystallized into an anatase phase during this process. SiO_2/TiO_2-NSs embedded with gold, silver, and platinum nanoparticles were prepared similarly with ap-SiO_2-NSs embedded with the corresponding metal nanoparticles.

Preparation of hollow titania nanosheets (et-TiO_2-NSs)

The SiO_2 in SiO_2/TiO_2-NSs was removed by chemical etching with NaOH solution. SiO_2/TiO_2-NSs after calcination (ca-SiO_2/TiO_2-NSs) were dispersed into 6 mL deionized water, and then 2 mL 2 mol L^{-1} NaOH aqueous solution was added. The mixture was stirred and equilibrated at 60 °C for 4 h, and then et-TiO_2-NSs were obtained and collected by centrifugation and washed with deionized water. et-TiO_2-NSs embedded with gold, silver, and platinum nanoparticles were prepared similarly with ca-SiO_2/TiO_2-NSs embedded with the corresponding metal nanoparticles.

Photocatalytic experiments

The photocatalytic properties of the samples were examined by measuring the decomposition rate of methyl orange (MO) in the presence of the photocatalyst under light irradiation of a 300 W Xe lamp (no cut-off filter was used). Briefly, 5 mg of SiO_2/TiO_2-NSs or Au/SiO_2/TiO_2-NSs powder was added to 10 mL of MO

 This journal is © The Royal Society of Chemistry 2013

Published on 14 May 2013. Downloaded by Shanghai Jiaotong University on 01/11/2013 10:41:38.

aqueous solution (0.05 mM). Before illumination, the solution was slightly stirred for 120 min in the dark to reach an adsorption equilibrium, and then photocatalytic degradation was monitored by measuring the absorption of the solution using a UV-2550 spectrophotometer (Shimadzu, Japan). At given intervals of illumination time, the samples of the reaction solution were taken out and analyzed.

Characterization

Fourier transform infrared absorption spectra (FTIR). FTIR measurements were carried out with an iS10 Fourier transformation infrared absorption spectrometer (Nicolet, USA). The samples were prepared with a KBr disk.

Thermogravimetric analysis (TGA). TGA was performed in nitrogen at a heating rate of 20 °C min^{-1} from 100 °C to 700 °C using a TA Q5000IR thermogravimetric analyzer. For each measurement the sample cell was maintained at 100 °C for 5 min to evaporate the solvent in the sample before measurement.

Transmission electron microscopy (TEM), selected area electron diffraction (SAED) and high resolution transmission electron microscopy (HRTEM). The TEM images, SAED patterns, and HRTEM images were all obtained using a JEM-2100 (JEOL Ltd., Japan) transmission electron microscope operated at an acceleration voltage of 200 kV. The samples were prepared by dropping an ethanol dispersion of the nanosheets onto copper grids coated with a thin polymer film and then drying at room temperature.

Scanning transmission electron microscopy (STEM) and energy dispersive spectroscopy (EDS). The STEM images and STEM-EDS mapping of each element were obtained using a JEM-2100F (JEOL Ltd., Japan) transmission electron microscope operated at an acceleration voltage of 200 kV equipped with an Oxford Instruments EDS detector. The samples were prepared similarly to the TEM samples. Some of the samples were also sliced with a Leica Ultracut UC6 low temperature sectioning system and transferred onto copper grids to observe the cross-section of the nanosheets.

Scanning electron microscopy (SEM). The SEM images were obtained using a JSM-7401F (JEOL Ltd., Japan) field emission scanning electron microscope operated at an acceleration voltage of 5 kV. The samples were prepared by dropping an ethanol dispersion of the nanosheets onto silica wafers and drying at room temperature. The samples were then sputter-coated with gold to minimize charging.

Wide-angle X-ray diffraction (XRD). XRD experiments were performed at room temperature on a glass slide using a Rigaku X-ray diffractometer D/MAX-2200/PC with a rotating anode source operated at 40 kV and 20 mA, and the spectra were recorded in the scattering angle (2θ) range of 5–80° (step size 0.02°). Cu Kα radiation with wavelength $\lambda = 0.1542$ nm was used for the measurements.

X-Ray photoelectron spectroscopy (XPS). XPS experiments were carried out on a RBD upgraded PHI-5000C ESCA system (Perkin Elmer) with Al Kα radiation ($h\nu = 1486.6$ eV). The X-ray anode was run at 250 W and a high voltage was kept at 14.0 kV with a detection angle at 54°. Binding energies were calibrated by using the containment carbon (C 1s = 284.6 eV). The samples were directly pressed into disks before measurement. The data analysis was carried out by using the RBD AugerScan 3.21 software provided by RBD Enterprises.

X-Ray fluorescence spectroscopy (XRF). XRF experiments were carried out on a XRF-1800 sequential X-ray fluorescence spectrometer (Shimadzu, Japan). The samples were directly pressed into disks before measurement.

Nitrogen adsorption–desorption analysis. Nitrogen adsorption–desorption isotherms were determined at 77 K using an ASAP 2010 M+C surface area and porosimetry analyzer (Micromeritics Inc., USA). The specific surface areas were calculated according to the Brunauer–Emmett–Teller (BET) method in regions applicable to the derivation of the model between P/P_0 values of 0.05–0.25, and the pore volumes and pore size distributions were obtained using the Barrett–Joyner–Halenda (BJH) model. The total pore volume was estimated from the uptake of nitrogen at a relative pressure of $P/P_0 = 0.99$.

Results and discussion

The whole strategy to prepare the SiO_2/TiO_2-NSs is illustrated in Scheme 1. As templates, hPEA-NSs possess a sandwich-like structure, which is comprised of the hydrophilic outer layer of hPEA and the hydrophobic crosslinked inner layer of POSS and AN moieties.[35] Because cationic polymers can promote localized silica deposition, the amino groups in the outer layer of hPEA-NSs can facilitate the heterogeneous nucleation process of the precursor of SiO_2 (TEOS) around the surface of hPEA-NSs rather than a homogeneous nucleation process in bulk solution. As a result, TEOS can be immobilized into the hydrophilic outer layer of hPEA-NSs to form subsequently silica nanosheets (SiO_2-NSs) by a hydrolysis step. After the formation of SiO_2-NSs, the precursor of TiO_2 (TBT) was then added and deposited on the surface of SiO_2-NSs through a sol–gel reaction to form SiO_2/TiO_2-NSs. After calcination at 300–600 °C, the hPEA-NSs template was removed while the amorphous TiO_2 in the nanosheets partly crystallized into the anatase phase during this process.

The morphology of the obtained SiO_2-NSs and SiO_2/TiO_2-NSs was first observed using transmission electron microscopy (TEM) and scanning electron microscopy (SEM) (Fig. 1). As shown in Fig. 1b, the as-prepared SiO_2-NSs (ap-SiO_2-NSs) maintained the square sheet morphology of the hPEA-NSs (Fig. 1a) with edge lengths of 1–2 μm, and the thickness of the ap-SiO_2-NSs was ~20 nm measured from the wrinkles of the nanosheets shown in the TEM image (Fig. 1b). The TiO_2 phase was deposited on the SiO_2-NSs, and the morphology of the as-prepared SiO_2/TiO_2-NSs (ap-SiO_2/TiO_2-NSs) could still maintain the square shape (Fig. 1c and d) while the thickness of the nanosheets was ~51 nm, determined by the SEM images. After calcination, no obvious aggregation occurred, as shown in the SEM image (Fig. 1e), while the thickness of the SiO_2/TiO_2-NSs after calcination (ca-SiO_2/TiO_2-NSs) was ~46 nm, determined by the SEM images. The thickness of

Published on 14 May 2013. Downloaded by Shanghai Jiaotong University on 01/11/2013 10:41:38.

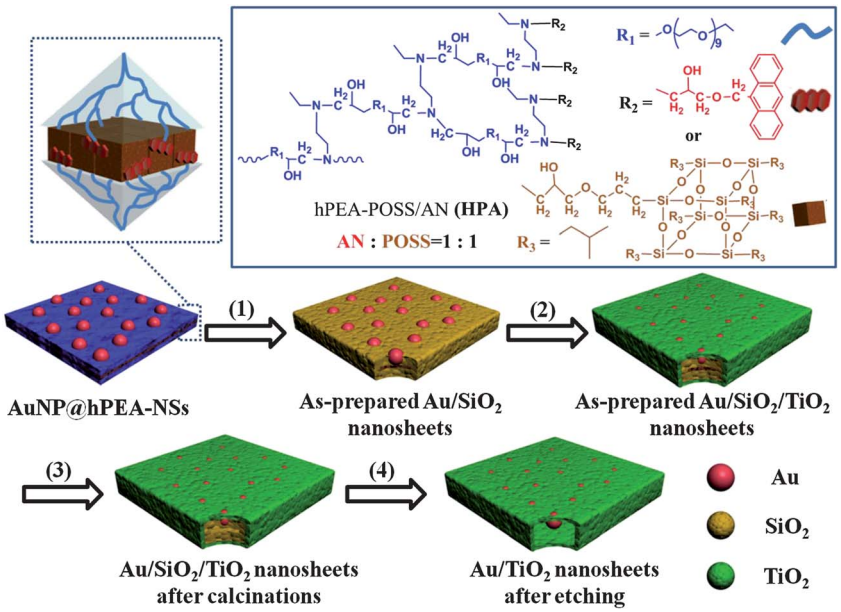

Scheme 1 The structure of POSS/AN ended hPEA which can self-assemble into hybrid nanosheets and the strategy to prepare the SiO_2/TiO_2-NSs embedded with metal nanoparticles (for example, gold nanoparticles): (1) hydrolysis, TEOS, ethanol–water, 24 h. (2) Hydrolysis, TBT, ethanol, 24 h. (3) Calcination, 30–300–600 °C, 4 h. (4) Etching, 2 mol L^{-1} NaOH, 4 h.

SiO_2/TiO_2-NSs decreased after calcination, which might be ascribed to the shrinking of the nanosheets caused by the removal of the hPEA-NS template. The aspect ratio between the edge length and the thickness of the obtained nanosheets is about 30, which is larger than some of the reports.[43,44] The TEM image of ca-SiO_2/TiO_2-NSs was shown in Fig. 1f and g, and some darker spots appeared in the surface of the nanosheets after calcination, which were due to the condensation of some smaller crystallites.[18] Meanwhile, the amorphous TiO_2 in the nanosheets crystallized into anatase phase after calcination, which was proven by the HRTEM image and SAED pattern in Fig. 1h. The HRTEM image of ca-SiO_2/TiO_2-NSs shows a clear crystal lattice with uniform interplanar spacings of 0.35 nm and 0.23 nm, which correspond to the (101) and (004) planes of the anatase phase, respectively. The SAED pattern of the ca-SiO_2/TiO_2-NSs exhibits diffraction rings, which correspond to the (101), (004), (200), (105), (204), (116), (220), and (215) planes of anatase TiO_2, respectively. All these results could also be regarded as a proof for the anatase phase in ca-SiO_2/TiO_2-NSs. The TEM images in Fig. 1f and g also indicated that the TiO_2 phase on the surface of ca-SiO_2/TiO_2-NSs consisted of numerous discrete anatase nanoparticles with diameters of 6–8 nm and these hierarchical architectured nanosheets also possessed mesoscale disordered pores. The successful preparation of SiO_2-NSs and SiO_2/TiO_2-NSs can also be confirmed by Fourier transform infrared absorption spectra (FTIR), as shown in Fig. S1.†

Then SiO_2-NSs and SiO_2/TiO_2-NSs embedded with AuNPs (Au/SiO_2-NSs and Au/SiO_2/TiO_2-NSs) were prepared similarly with hPEA-NSs decorated with AuNPs (AuNP@hPEA-NSs) as templates and the morphology of these obtained nanosheets was also investigated by TEM and SEM (Fig. 2). As shown in Fig. 2b–e, Au/SiO_2-NSs and Au/SiO_2/TiO_2-NSs could also maintain the square sheet morphology of the template AuNP@hPEA-NSs, and nearly no crush or aggregation was observed in the SEM images even after calcination. Meanwhile, most of AuNPs could be fixed on the nanosheets during the preparation, which was revealed by the TEM images shown in Fig. 2d and f. The successful embedding of AuNPs into the nanosheets could also be indicated by the pink color of Au/SiO_2/TiO_2-NSs, which was attributed to the characteristic plasmonic absorption of AuNPs.

The sandwich-like structure of ca-Au/SiO_2/TiO_2-NSs which is comprised of amorphous SiO_2 as the inner layer and the anatase TiO_2 as the outer layer was confirmed by the scanning transmission electron microscopy (STEM) image and energy dispersive spectroscopy (EDS) spectrum of both the surface and cross-section. As shown in Fig. 3c, the silicon, titanium, and oxygen elements have almost the same distribution, which indicates that the TiO_2 phase is deposited homogeneously on the surface of the SiO_2 phase. The EDS mapping of the cross-section of ca-Au/SiO_2/TiO_2-NSs in Fig. 3d exhibits that the distributions of silicon and titanium elements are complementary; the TiO_2 phase is distributed at the outer layer of the nanosheets while the SiO_2 phase is at the inner layer, which is well consistent with the sandwich structure predicted in Scheme 1. It's also shown in Fig. 3d that the thickness of ca-Au/SiO_2/TiO_2-NSs is ~40 nm while the SiO_2 layer in the nanosheet is ~20 nm, which is also in agreement with the thicknesses of SiO_2-NSs and SiO_2/TiO_2-NSs determined by the TEM and SEM images in Fig. 1. Moreover, the distribution of elemental gold is also exhibited in EDS mapping of ca-Au/SiO_2/TiO_2-NSs, suggesting the existence of AuNPs embedded in the nanosheets.

 This journal is © The Royal Society of Chemistry 2013

Published on 14 May 2013. Downloaded by Shanghai Jiaotong University on 01/11/2013 10:41:38.

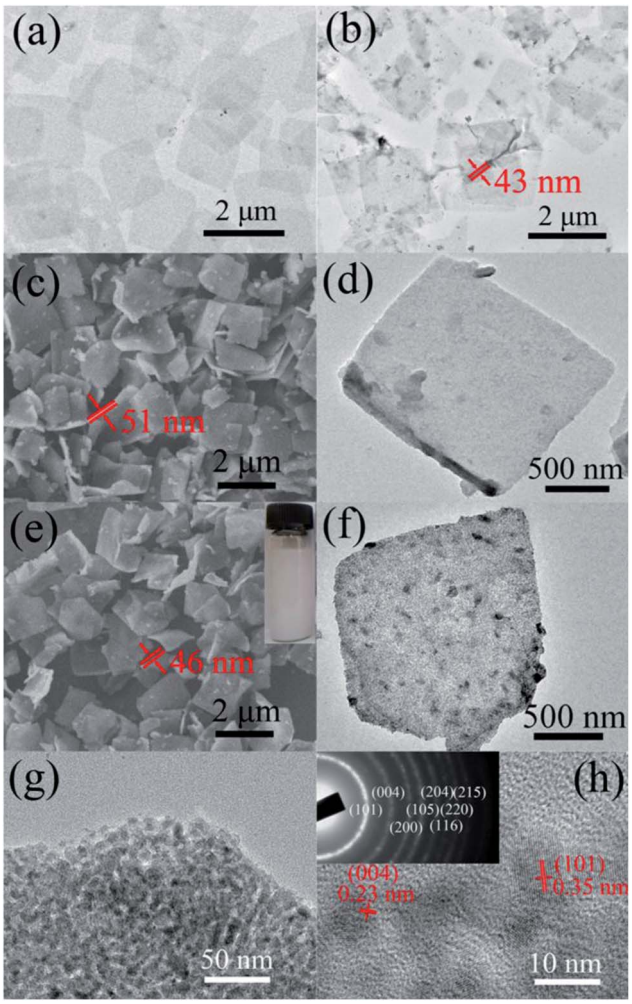

Fig. 1 TEM images (a, b, d, f and g) and SEM images (c and e) of hPEA-NSs (a), ap-SiO_2-NSs (b), ap-SiO_2/TiO_2-NSs (c and d), ca-SiO_2/TiO_2-NSs (e, f and g), respectively. (h) HRTEM image of ca-SiO_2/TiO_2-NSs, inset: SAED pattern of ca-SiO_2/TiO_2-NSs. Inset (e): the digital photograph of ca-SiO_2/TiO_2-NSs dispersed in ethanol.

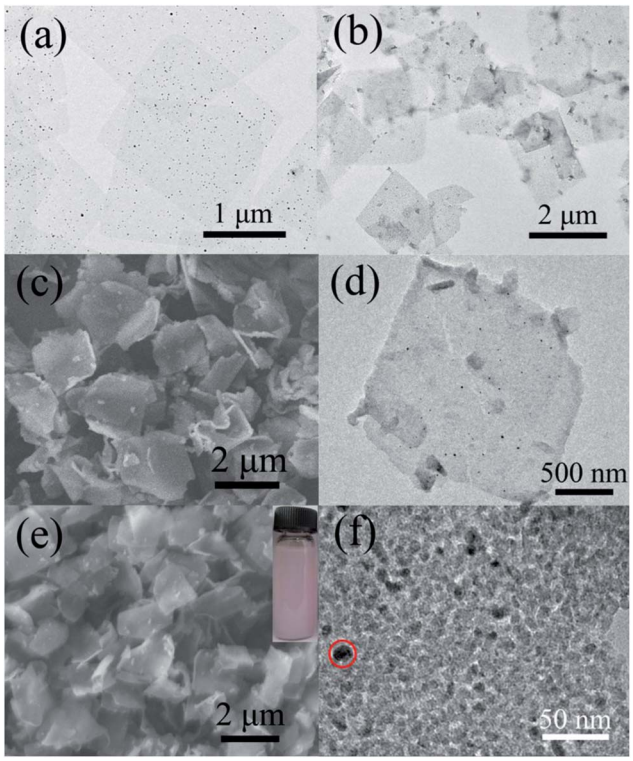

Fig. 2 TEM images (a, b, d and f) and SEM images (c and e) of hPEA-NSs decorated with AuNPs (AuNP@hPEA-NSs) (a), ap-Au/SiO_2-NSs (b), ap-Au/SiO_2/TiO_2-NSs (c and d), ca-SiO_2/TiO_2-NSs (e and f), respectively, and AuNPs was marked in (f). Inset (e): the digital photograph of ca-Au/SiO_2/TiO_2-NSs dispersed in ethanol.

In order to determine the detailed composition of the Au/SiO_2/TiO_2-NSs, thermogravimetric analysis (TGA), X-ray photoelectron spectroscopy (XPS), and X-ray fluorescence spectroscopy (XRF) experiments were carried out, and the results are shown in Fig. S2 and S3.† The weight percentages of SiO_2, TiO_2, and Au calculated through the XPS and XRF results are summarized in Table 1. The weight percentages of SiO_2 and TiO_2 in ca-SiO_2/TiO_2-NSs are 37.9% and 62.1%, respectively, which is very close to the theoretical value from the TEOS and TBT in-feed (38.1% and 61.9%). The amount of Au element obtained from XRF is much larger than that determined by XPS. This result might be ascribed to the fact that most AuNPs are distributed at the inner layer of the nanosheets, which is consistent with the STEM image and EDS mapping in Fig. 3d.

The crystal structure and phase of these nanosheets were investigated by wide-angle X-ray diffraction (XRD) (Fig. 4). In XRD spectra of nanosheets embedded with AuNPs, the embedding of AuNPs could also be demonstrated by the common pattern of a face-centered cubic gold lattice at 2θ = 38°, 44°, 64°, and 78°, respectively. Moreover, well-developed Bragg reflection attributed to the anatase TiO_2 phase appeared in the XRD spectra of SiO_2/TiO_2-NSs after calcination, suggesting the phase transition of amorphous TiO_2 to anatase TiO_2. Compared with those of the bulk counterpart, the peaks were relatively broadened, which demonstrated the small size of the anatase TiO_2 nanoparticles.[18] No characteristic diffraction peaks attributed to rutile TiO_2 appeared in the spectra, which was also consistent with the HRTEM image and SAED pattern of ca-SiO_2/TiO_2-NSs in Fig. 1h. The particle size of the anatase TiO_2 nanocrystals in these calcined nanosheets was ~7 nm, calculated using the Scherrer equation,[45] which was also in agreement with the diameter determined from the TEM image in Fig. 1g.

The surface area and pore structure of these nanosheets after calcination were investigated by using N_2 adsorption–desorption isotherm measurements. As shown in Fig. 5a, ca-SiO_2-NSs and ca-SiO_2/TiO_2-NSs both presented BDDT type IV shapes of isotherms, according to IUPAC classification, associated with a well-defined capillary condensation step suggesting a mesoporous structure.[46,47] Moreover, the volume adsorbed was larger at high relative pressure, exhibiting the H3-type hysteresis loop, and this kind of hysteresis loop indicated that ca-SiO_2-NSs and ca-SiO_2/TiO_2-NSs are both comprised of aggregates of plate-like

Published on 14 May 2013. Downloaded by Shanghai Jiaotong University on 01/11/2013 10:41:38.

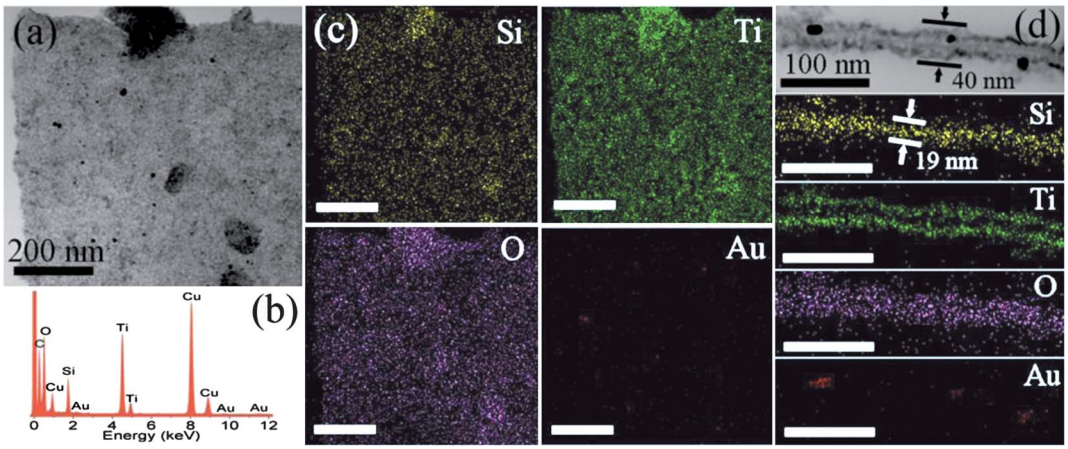

Fig. 3 The STEM image (a), EDS spectrum (b), and EDS mappings (c) of ca-Au/SiO_2/TiO_2-NSs; inset scale bar is 200 nm. (d) The STEM image and EDS mapping of the cross-section of ca-Au/SiO_2/TiO_2-NSs, inset scale bar is 100 nm.

Table 1 The composition of the ca-SiO_2/TiO_2-NSs, ca-Au/SiO_2/TiO_2-NSs, and et-Au/TIO_2-NSs measured by XPS and XRF

	Weight percentage by XPS (%)			Weight percentage by XRF (%)		
Sample	SiO_2	TiO_2	AuNP	SiO_2	TiO_2	AuNP
ca-SiO_2/TiO_2-NSs	37.9	62.1	—	35.2	64.8	—
ca-Au/SiO_2/TiO_2-NSs	37.2	62.1	0.7	31.3	65.2	3.5
et-Au/TiO_2-NSs	8.4	90.4	1.2	—	—	—

particles forming slit-like pores.[48,49] The BET specific surface areas of the samples were listed in Table 2, which exhibited ca-SiO_2-NSs possessing a very high BET specific surface area of 618.8 m^2 g^{-1}. This result was comparable to the values reported for conventional mesoporous silica.[32,50] Meanwhile, the BET surface areas and the total pore volume of pores of ca-SiO_2/TiO_2-NSs were also measured, which had decreased after the deposition of TiO_2. The embedding of AuNPs had little effect on the BET surface areas and total pore volumes, which was also exhibited in Table 2. The pore size distribution was further analyzed based on the BJH method, and the results were shown in Fig. 5b. The average pore diameters of ca-SiO_2-NSs and ca-SiO_2/TiO_2-NSs were 8.43 nm and 4.94 nm, respectively (Table 2), which had decreased after the deposition of TiO_2 layers. This phenomenon might be ascribed to the fact that that ca-SiO_2-NSs possessed pores with two different average diameters, as shown in Fig. 5b, and most of the larger pores (~16 nm) were filled with TiO_2 nanoparticles (~7 nm) during the TiO_2 layer deposition process, resulting in the decrease of the pore size of ca-SiO_2/TiO_2-NSs compared with ca-SiO_2-NSs.

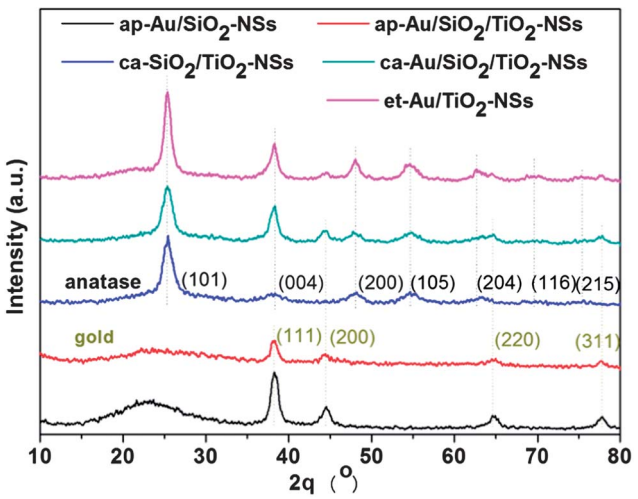

Fig. 4 The XRD spectra of ap-Au/SiO_2-NSs, ap-Au/SiO_2/TiO_2-NSs, ca-SiO_2/TiO_2-NSs, ca-Au/SiO_2/TiO_2-NSs and et-Au/TiO_2-NSs, respectively.

In our previous research, the diameters and densities of AuNPs decorated on hPEA-NSs template can be tunable by the amount of $HAuCl_4$ in the feed.[36] As a result, we could also change the density of AuNPs embedded into SiO_2/TiO_2-NSs through the same method. In addition, AgNPs and PtNPs could also be embedded into SiO_2/TiO_2-NSs similarly to AuNPs. Fig. 6 presents the SEM and TEM images of ca-SiO_2/TiO_2-NSs embedded with different types of metal nanoparticles, which indicated that all these nanosheets could maintain the square sheet morphology of the hPEA-NSs templates and nearly no aggregation occurred during calcination. Meanwhile, these metal nanoparticles embedded in the nanosheets could be easily observed from the magnified TEM images in Fig. 6, suggesting the successful embedding of AuNPs, AgNPs, and PtNPs in SiO_2/TiO_2-NSs, respectively, which was also consistent with the color changes of the corresponding nanosheets dispersed in ethanol shown in Fig. 6.

The inner SiO_2 layer of ca-Au/SiO_2/TiO_2-NSs could be removed by chemical etching with NaOH solution,[45,51] and anatase TiO_2 nanosheet-like boxes embedded with AuNPs (et-Au/TiO_2-NSs) could be obtained. This process was illustrated in Scheme 1. The successful etching of SiO_2 was proven by FT-IR (Fig. S1) and XPS (Fig. S3) spectra, and the morphology of et-Au/TiO_2-NSs was also investigated by SEM and TEM. As shown in Fig. 7a, most of the et-Au/TiO_2-NSs still maintained

 This journal is © The Royal Society of Chemistry 2013

Published on 14 May 2013. Downloaded by Shanghai Jiaotong University on 01/11/2013 10:41:38.

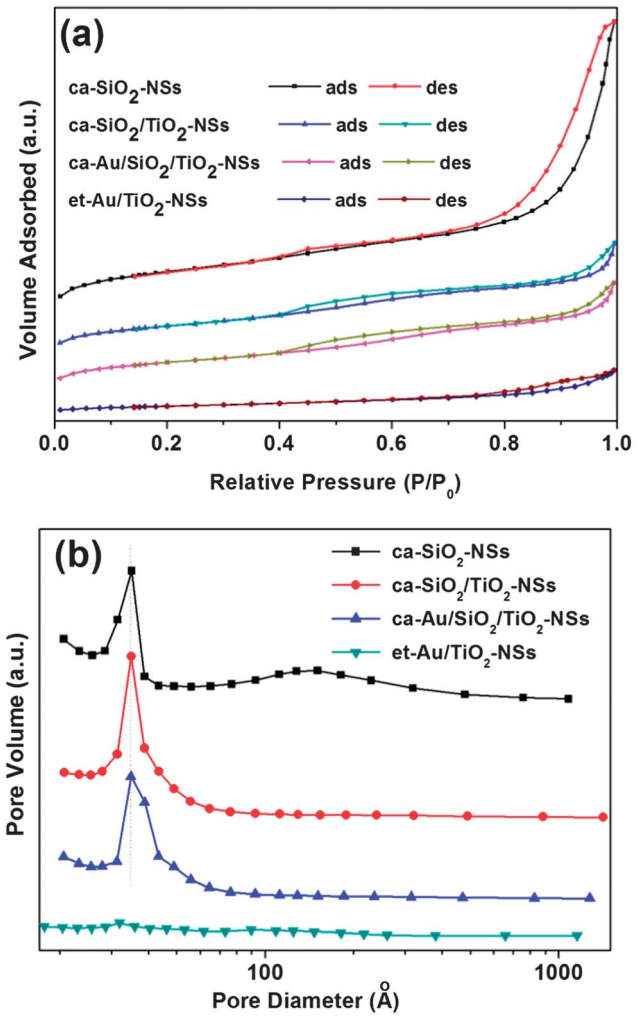

Fig. 5 N_2 adsorption–desorption isotherms (a) and pore size distribution curves (b) of ca-SiO_2-NSs, ca-SiO_2/TiO_2-NSs, ca-Au/SiO_2/TiO_2-NSs, and et-Au/TiO_2-NSs, respectively.

the square sheet morphology and large aspect ratio of ca-Au/SiO_2/TiO_2-NSs, and only a little deformation and aggregation was observed. No fusion occurred between the anatase TiO_2 nanoparticles deposited on the nanosheets (Fig. 7b). Compared with Fig. 3b, the silicon element content of et-Au/TiO_2-NSs determined by the EDS spectrum in Fig. 7d decreased from 5.06% to 0.72% (weight percentage), and the density of silicon element exhibited in EDS mapping of et-Au/TiO_2-NSs (Fig. 7e) also sharply decreased compared with Fig. 3c. All these results also confirmed that most of the SiO_2 in et-Au/TiO_2-NSs was removed. In fact, et-Au/TiO_2-NSs were composed of only 8.4% weight percentage of SiO_2 determined by XPS. As some of the amorphous TiO_2 in ca-Au/SiO_2/TiO_2-NSs could be also removed together with SiO_2 by etching with NaOH solution, the degree of crystallinity of the anatase phase in et-Au/TiO_2-NSs also increased during chemical etching. As shown in Fig. 4, the XRD peak of anatase TiO_2 in et-Au/TiO_2-NSs became sharper after etching. Meanwhile, the BET specific surface area and the total pore volume of pores of et-Au/TiO_2-NSs determined by N_2 adsorption–desorption

Table 2 Some physical characteristics of the ca-SiO_2-NSs, ca-SiO_2/TiO_2-NSs, ca-Au/SiO_2/TiO_2-NSs, and et-Au/TIO_2-NSs

Sample	S_{BET}[a]/m^2 g^{-1}	V_t[b]/cm^3 g^{-1}	Pore size[c]/nm
ca-SiO_2-NSs	618.8	1.304	8.43
ca-SiO_2/TiO_2-NSs	429.4	0.530	4.94
ca-Au/SiO_2/TiO_2-NSs	403.6	0.508	5.04
et-Au/TIO_2-NSs	75.1	0.179	9.55

[a] BET specific surface area was calculated from the linear part of the BET plot. [b] V_t = total pore volume of pores at P/P_0 = 0.99. [c] The average pore diameter was estimated from the Barrett–Joyner–Halenda (BJH) formula.

isotherms decreased after etching of SiO_2 (Table 2). Moreover, as shown in Fig. 5a, the N_2 adsorption–desorption isotherm of et-Au/TiO_2-NSs also exhibited an H3-type hysteresis loop, which indicated that et-Au/TiO_2-NSs were also comprised of plate-like particles forming slit-like pores. The hysteresis loop appeared at higher relative pressure, which is consistent with larger average pore size of et-Au/TiO_2-NSs after etching of SiO_2.

The photocatalysis behavior of TiO_2 has been most intensively investigated owing to its low cost, high chemical inertness, and environmental applications. The photocatalytic efficiency of TiO_2 can be affected by the size, shape, crystallinity, and degree of exposure of the reactive crystal facets.[43] It's also reported that increasing the surface area of TiO_2 can efficiently increase the surface adsorption capacity of the reactants, leading to the enhancement of photocatalytic reactions.[52] As a result, a variety of methods have been carried out to increase the surface area of TiO_2, such as synthesis of mesoporous TiO_2, deposition of TiO_2 on the surface of graphene,[46] MoS_2 nanosheets,[53] or carbon fibers,[54] and combination of TiO_2 with absorbents (for example, mesoporous SiO_2),[55,56] as well as direct synthesis of TiO_2 nanosheets.[43,44] Another promising route to enhance the photocatalytic performance of TiO_2 is to decorate the surface with metal nanoparticles (for example, Ag, Au, Pt and Pd).[57–59] It has been shown that the presence of the metal nanoparticles can efficiently shift the Fermi level of TiO_2, which results in enhanced photocatalytic efficiency.[60] The photocatalytic activity of ca-SiO_2/TiO_2-NSs, ca-Au/SiO_2/TiO_2-NSs, and et-Au/TiO_2-NSs were all evaluated by monitoring the degradation of Methyl Orange (MO) under Xe lamp irradiation. The changes of the MO concentration *versus* light irradiation time in presence of ca-SiO_2/TiO_2-NSs, ca-Au/SiO_2/TiO_2-NSs, and et-Au/TiO_2-NSs were summarized in Fig. 8. The mixtures containing the catalysts and MO were equilibrated in the dark for 120 min before irradiation to ensure the saturated adsorption of MO on the surface of the catalysts. As shown in Fig. 8, only ~4% C/C_0 of MO was decomposed after light irradiation for 120 min without catalyst. However, the degradation rates were significantly enhanced in presence of the nanosheets we prepared. The relative photocatalytic activity of ca-Au/SiO_2/TiO_2-NSs for MO degradation was higher than that of ca-SiO_2/TiO_2-NSs, which may be ascribed to the fact that MO photodegradation was enhanced by the localized surface plasmon resonance (LSPR) effect from AuNPs as it was irradiated by visible light.[57]

Published on 14 May 2013. Downloaded by Shanghai Jiaotong University on 01/11/2013 10:41:38.

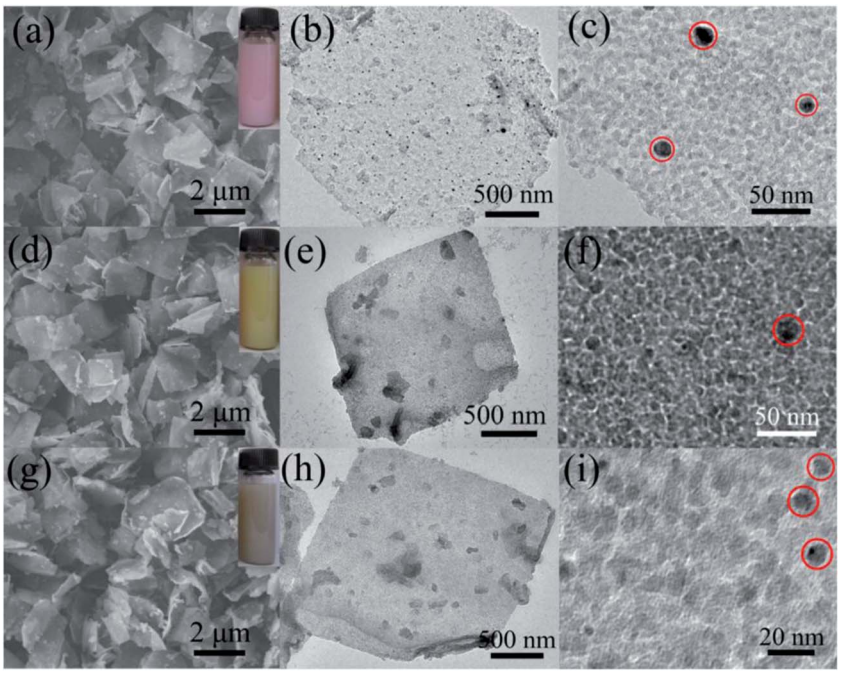

Fig. 6 SEM images (a, d and g) and TEM images (b, c, e, f, h and i) of ca-Au/SiO_2/TiO_2-NSs embedded with more AuNPs (a, b and c), ca-Ag/SiO_2/TiO_2-NSs (d, e and f), and ca-Pt/SiO_2/TiO_2-NSs (g, h and i). Inset: the digital photograph of the corresponding nanosheets dispersed in ethanol, and AuNPs, AgNPs, and PtNPs were marked in (c), (f), and (i), respectively.

In addition, et-Au/TiO_2-NSs showed a higher catalytic activity than ca-Au/SiO_2/TiO_2-NSs, which might be because of the AuNPs becoming more accessible to light after the SiO_2 etching process. Compared with P25 and some of the other mesoporous TiO_2, et-Au/TiO_2-NSs exhibited a comparable catalytic activity.[51,59]

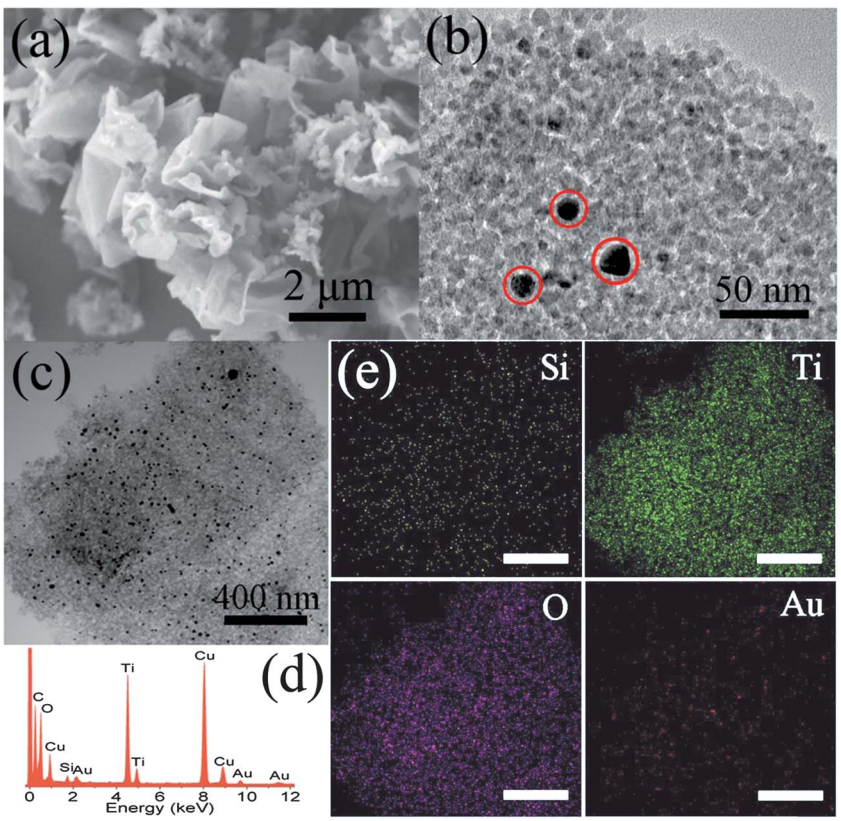

Fig. 7 SEM image (a), TEM image (b), STEM image (c), EDS spectrum (d), and EDS mappings (e) of et-Au/TiO_2-NSs, and AuNPs was marked in (b).

This journal is © The Royal Society of Chemistry 2013

Published on 14 May 2013. Downloaded by Shanghai Jiaotong University on 01/11/2013 10:41:38.

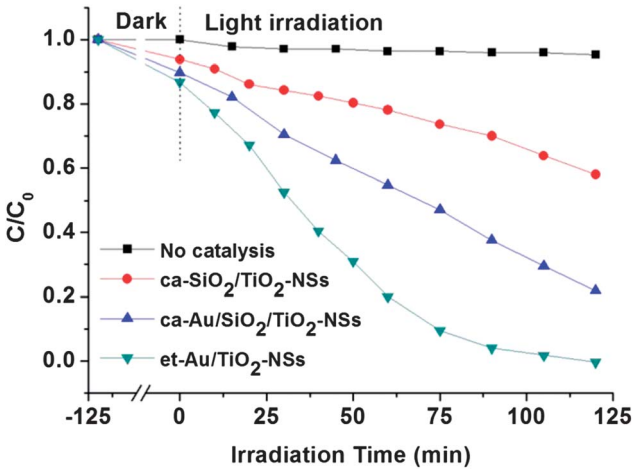

Fig. 8 The dependence of the MO concentration on 300 W Xe lamp irradiation time in the presence of different catalysts.

Conclusions

We have developed a novel approach to fabricate square silica/titania mesoporous nanosheets by using polymer nanosheets of hyperbranched poly(ether amine) as templates. The obtained nanosheets possess a large aspect ratio (~30), mesoporous structure, high surface area (~429 m^2 g^{-1}), and sandwich-like nanostructure, which is comprised of amorphous SiO_2 as the inner layer and anatase TiO_2 as the outer layer. AuNPs, AgNPs, and PtNPs can be embedded into the obtained nanosheets by using hPEA-NSs decorated with the corresponding nanoparticles as a template. Meanwhile, a further etching step of the inner silica layer in these nanosheets embedded with AuNPs can yield anatase TiO_2 nanosheet-like boxes embedded with AuNPs, which show significantly enhanced photodegradation of organic dyes such as MO. These characteristics may be due to the LSPR effect from AuNPs under the irradiation of visible light. To the best of our knowledge, hPEA-NSs were the first example of polymer nanosheets which were used as templates for fabrication of 2D inorganic materials. This approach to prepare inorganic mesoporous nanosheet templated by hPEA-NSs is believed to provide an alternative to produce various square inorganic mesoporous nanosheets with a large aspect ratio.

Acknowledgements

We thank the National Nature Science Foundation of China (21174085, 21274088), Science & Technology and Education Commission of Shanghai Municipal Government (11QA1403100, 12ZZ020), and the Shanghai Leading Academic Discipline Project (B202) for their financial support. X. S. Jiang is supported by the NCET-12-3050 Project.

References

1 C. Chao, Z. Ren, Y. Zhu, Z. Xiao, Z. Liu, G. Xu, J. Mai, X. Li, G. Shen and G. Han, *Angew. Chem., Int. Ed.*, 2012, **51**, 9283.
2 K. S. Novoselov, Z. Jiang, Y. Zhang, S. V. Morozov, H. L. Stormer, U. Zeitler, J. C. Maan, G. S. Boebinger, P. Kim and A. K. Geim, *Science*, 2007, **315**, 1379.
3 F. Schedin, A. K. Geim, S. V. Morozov, E. W. Hill, P. Blake, M. I. Katsnelson and K. S. Novoselov, *Nat. Mater.*, 2007, **6**, 652.
4 M. D. Stoller, S. Park, Y. Zhu, J. An and R. S. Ruoff, *Nano Lett.*, 2008, **8**, 3498.
5 J. W. Seo, Y. W. Jun, S. W. Park, H. Nah, T. Moon, B. Park, J. G. Kim, Y. J. Kim and J. Cheon, *Angew. Chem., Int. Ed.*, 2007, **46**, 8828.
6 R. J. Smith, P. J. King, M. Lotya, C. Wirtz, U. Khan, S. De, A. O'Neill, G. S. Duesberg, J. C. Grunlan, G. Moriarty, J. Chen, J. Wang, A. I. Minett, V. Nicolosi and J. N. Coleman, *Adv. Mater.*, 2011, **23**, 3944.
7 A. Yella, E. Mugnaioli, M. Panthöfer, U. Kolb and W. Tremel, *Angew. Chem., Int. Ed.*, 2010, **49**, 3301.
8 D. Wang, Y. Kang, V. Doan-Nguyen, J. Chen, R. Küngas, N. L. Wieder, K. Bakhmutsky, R. J. Gorte and C. B. Murray, *Angew. Chem., Int. Ed.*, 2011, **50**, 4378.
9 C. Schliehe, B. H. Juarez, M. Pelletier, S. Jander, D. Greshnykh, M. Nagel, A. Meyer, S. Foerster, A. Kornowski, C. Klinke and H. Weller, *Science*, 2010, **329**, 550.
10 Y. Omomo, T. Sasaki, L. Z. Wang and M. Watanabe, *J. Am. Chem. Soc.*, 2003, **125**, 3568.
11 H. Zhong, G. Yang, H. Song, Q. Liao, H. Cui, P. Shen and C. X. Wang, *J. Phys. Chem. C*, 2012, **116**, 9319.
12 Y. Hu, Z. Zheng, H. Jia, Y. Tang and L. Zhang, *J. Phys. Chem. C*, 2008, **112**, 13037.
13 P. Hu, L. Wang, M. Yoon, J. Zhang, W. Feng, X. Wang, Z. Wen, J. C. Idrobo, Y. Miyamoto, D. B. Geohegan and K. Xiao, *Nano Lett.*, 2013, **13**(4), 1649–1654.
14 W. Li and D. Zhao, *Adv. Mater.*, 2013, **25**, 142.
15 A. Khanal, Y. Inoue, M. Yada and K. Nakashima, *J. Am. Chem. Soc.*, 2007, **129**, 1534.
16 J. Yang, J. U. Lind and W. C. Trogler, *Chem. Mater.*, 2008, **20**, 2875.
17 M. Müllner, T. Lunkenbein, N. Miyajima, J. Breu and A. H. E. Müller, *Small*, 2012, **8**, 2636.
18 M. Müllner, T. Lunkenbein, M. Schieder, A. H. Gröschel, N. Miyajima, M. Förtsch, J. Breu, F. Caruso and A. H. E. Müller, *Macromolecules*, 2012, **45**, 6981.
19 K. Jiang, A. Eitan, L. S. Schadler, P. M. Ajayan, R. W. Siegel, N. Grobert, M. Mayne, M. Reyes-Reyes, H. Terrones and M. Terrones, *Nano Lett.*, 2003, **3**, 275.
20 P. M. Ajayan, O. Stephan, P. Redlich and C. Colliex, *Nature*, 1995, **375**, 564.
21 J. Xie, Y. Duan and S. Che, *Adv. Funct. Mater.*, 2012, **22**, 3784.
22 W. Shenton, T. Douglas, M. Young, G. Stubbs and S. Mann, *Adv. Mater.*, 1999, **11**, 253.
23 E. Dujardin, C. Peet, G. Stubbs, J. N. Culver and S. Mann, *Nano Lett.*, 2003, **3**, 413.
24 H. Zhou, X. Li, T. Fan, F. E. Osterloh, J. Ding, E. M. Sabio, D. Zhang and Q. Guo, *Adv. Mater.*, 2010, **22**, 951.
25 K. Chung, S. Yu, C. J. Heo, J. W. Shim, S. M. Yang, M. G. Han, H. S. Lee, Y. Jin, S. Y. Lee, N. Park and J. H. Shin, *Adv. Mater.*, 2012, **24**, 2375.

Published on 14 May 2013. Downloaded by Shanghai Jiaotong University on 01/11/2013 10:41:38.

26 J. Yuan, Y. Lu, F. Schacher, T. Lunkenbein, S. Weiss, H. Schmalz and A. H. E. Müller, *Chem. Mater.*, 2009, **21**, 4146.
27 J. Yuan, Y. Xu, A. Walther, S. Bolisetty, M. Schumacher, H. Schmalz, M. Ballauff and A. H. E. Müller, *Nat. Mater.*, 2008, **7**, 718.
28 M. Zhang, M. Drechsler and A. H. E. Müller, *Chem. Mater.*, 2004, **16**, 537.
29 J. Yuan, M. Drechsler, Y. Xu, M. Zhang and A. H. E. Müller, *Polymer*, 2008, **49**, 1547.
30 X. Shi, L. Pan, S. Chen, Y. Xiao, Q. Liu, L. Yuan, J. Sun and L. Cai, *Langmuir*, 2009, **25**, 5940.
31 M. Sasidharan, K. Nakashima, N. Gunawardhana, T. Yokoi, M. Inoue, S. I. Yusa, M. Yoshio and T. Tatsumi, *Chem. Commun.*, 2011, **47**, 6921.
32 S. Yang, X. Feng, L. Wang, K. Tang, J. Maier and K. Müllen, *Angew. Chem., Int. Ed.*, 2010, **49**, 4795.
33 Z. M. Wang, W. Wang, N. Coombs, N. Soheilnia and G. A. Ozin, *ACS Nano*, 2010, **4**, 7437.
34 Y. Chen, *Macromolecules*, 2012, **45**, 2619.
35 B. Yu, X. Jiang and J. Yin, *Macromolecules*, 2012, **45**, 7135.
36 B. Yu, X. Jiang and J. Yin, *Chem. Commun.*, 2013, **49**, 603.
37 G. Sauthier, E. György, A. Figueras, R. S. Sánchez and J. Hernando, *J. Phys. Chem. C*, 2012, **116**, 14534.
38 M. Ye, J. Gong, Y. Lai, C. Lin and Z. Lin, *J. Am. Chem. Soc.*, 2012, **134**, 15720.
39 T. Kiyonaga, T. Akita and H. Tada, *Chem. Commun.*, 2009, 2011.
40 H. Pang, H. Yang, C. X. Guo, J. Lu and C. M. Li, *Chem. Commun.*, 2012, **48**, 8832.
41 S. Liu, H. Jia, L. Han, J. Wang, P. Gao, D. Xu, J. Yang and S. Che, *Adv. Mater.*, 2012, **24**, 3201.
42 X. Zhang, A. Fujishima, M. Jin, A. V. Emeline and T. Murakami, *J. Phys. Chem. B*, 2006, **110**, 25142.
43 X. Han, Q. Kuang, M. Jin, Z. Xie and L. Zheng, *J. Am. Chem. Soc.*, 2009, **131**, 3152.
44 J. Zhang, J. Xi and Z. Ji, *J. Mater. Chem.*, 2012, **22**, 17700.
45 J. B. Joo, Q. Zhang, I. Lee, M. Dahl, F. Zaera and Y. Yin, *Adv. Funct. Mater.*, 2012, **22**, 166.
46 J. M. Lee, I. Y. Kim, S. Y. Han, T. W. Kim and S. J. Hwang, *Chem.–Eur. J.*, 2012, **18**, 13800.
47 Z. Zhai, C. Hu, X. Yang, L. Zhang, C. Liu, Y. Fan and W. Hou, *J. Mater. Chem.*, 2012, **22**, 19122.
48 L. Liu, X. Gu, C. Sun, H. Li, Y. Deng, F. Gao and L. Dong, *Nanoscale*, 2012, **4**, 6351.
49 W. Sun, S. Zhou, B. You and L. Wu, *Chem. Mater.*, 2012, **24**, 3800.
50 C. Dickinson, W. Zhou, R. P. Hodgkins, Y. F. Shi, D. Y. Zhao and H. Y. He, *Chem. Mater.*, 2006, **18**, 3088.
51 T. Leshuk, S. Linley, G. Baxter and F. Gu, *ACS Appl. Mater. Interfaces*, 2012, **4**, 6062.
52 S. K. Choi, S. Kim, S. K. Lim and H. Park, *J. Phys. Chem. C*, 2010, **114**, 16475.
53 W. Zhou, Z. Yin, Y. Du, X. Huang, Z. Zeng, Z. Fan, H. Liu, J. Wang and H. Zhang, *Small*, 2013, **9**, 140.
54 W. Guo, F. Zhang, C. Lin and Z. L. Wang, *Adv. Mater.*, 2012, **24**, 4761.
55 J. Bahadur, D. Sen, S. Mazumder, P. U. Sastry, B. Paul, H. Bhatt and S. G. Singh, *Langmuir*, 2012, **28**, 11343.
56 X. Li, V. T. John, G. He, J. He and L. Spinu, *J. Mater. Chem.*, 2012, **22**, 17476.
57 J. J. Chen, J. C. S. Wu, P. C. Wu and D. P. Tsai, *J. Phys. Chem. C*, 2012, **116**, 26535.
58 D. Tsukamoto, Y. Shiraishi, Y. Sugano, S. Ichikawa, S. Tanaka and T. Hirai, *J. Am. Chem. Soc.*, 2012, **134**, 6309.
59 G. Wang, X. Wang, J. Liu and X. Sun, *Chem.–Eur. J.*, 2012, **18**, 5361.
60 R. Su, R. Tiruvalam, Q. He, N. Dimitratos, L. Kesavan, C. Hammond, J. A. Lopez-Sanchez, R. Bechstein, C. J. Kiely, G. J. Hutchings and F. Besenbacher, *ACS Nano*, 2012, **6**, 6284.

 This journal is © The Royal Society of Chemistry 2013